Nuclear Engineering and Design 444 (2025) 114372

Contents lists available at ScienceDirect

Nuclear Engineering and Design

journal homepage: www.elsevier.com/locate/nucengdes

Off-centering effects on MOX fuel behavior☆

D. Jaramillo-Sierra [a,b,*], V. Blanc [c], T. Barani [c], A. Cammi [a], A. Del Nevo [b]

[a] Politecnico di Milano, Department of Energy, Nuclear Engineering Division, via La Masa 34, 20156 Milano, Italy
[b] ENEA, NUC-ING, Località Bacino del Brasimone 1, Camugnano, 40032 Bologna, Italy
[c] CEA, IRESNE, DEC, SESC, Cadarache Center, 13108 Saint-Paul-lez-Durance, France

ARTICLE INFO

Keywords:
Fuel performance
Off-centering
Eccentricity
PuMMA
TRANSURANUS
GERMINAL
MFEM
High plutonium mixed-oxide fuel
CAPRIX
TRABANT-2/2

ABSTRACT

Standard fuel performance models often assume concentric alignment of fuel pellets within the cladding, overlooking the potential effects of pellet eccentricity on reactor performance and safety. This paper investigates the thermal and porosity dynamics of hollow MOX fuel with off-centered pellets under irradiation, using a Finite Element Method (FEM) model implemented via the MFEM library. Simulations replicate experimental conditions from the PuMMA Horizon Europe project, considering the CAPRIX and TRABANT-2/2 experimental pins with high plutonium content MOX fuel. Results reveal that pellet eccentricity induces asymmetrical temperature peaks, significantly reducing the margin to melt compared to the results of axisymmetric modeling, and drives anisotropic pore migration, phenomena with critical implications for the safety and design of Gen-IV reactor fuels. Comparisons against post-irradiation examinations (PIE) confirm the model capability to semi-quantitatively replicate the observed behavior. These findings highlight the need to integrate pellet eccentricity into safety assessments and advanced fuel design strategies, especially for hollow fuels for Gen-IV reactors.

1. Introduction

The standard fuel performance analysis typically assumes axial symmetry of the fuel rod, with the fuel pellet remaining concentric relative to the cladding throughout irradiation. This assumption is largely based on studies of Light Water Reactors (LWRs), where solid pellet off-centering is found to have beneficial temperature effects (Cunningham et al., 1979). However, applying these results to advanced fuels for Generation IV reactors (Generation IV International Forum, 2014) requires careful consideration due to differences in geometry, irradiation conditions, and material properties.

Early studies by Nijsing (1966) first addressed the effect of off-centering on gap conductance, providing an analytical solution for a non-uniform heat generation distribution and exploring how fuel-cladding eccentricity influences gap conductance. Similarly, Williford and Hann (1977) demonstrated that eccentricity significantly increases the average gap conductance in cases of high thermal gradients across the gap.

Experimentally, Cunningham et al. (1979) studied the effects of pellet off-centering and gas composition on the fuel rod performance in two HALDEN reactor assemblies. They concluded that the eccentric region of a xenon-filled fuel rod exhibited lower temperatures than the concentric region, suggesting improved azimuthal average gap conductance.

Mcnary and Bauer (1981) indicate that centered pellets represent the minimum azimuthally average gap conductance, with asymmetrical conductance effects becoming more significant in high-conductivity fuels. In contrast, Tao et al. (2023) argue that eccentricity has a minimal impact on the safety of high-conductivity metal fuels. This is expected, as sodium-bonded metallic fuels exhibit a lower thermal gradient both within the fuel and across the gap, reducing the gap's relevance.

Wiesenack (1996) evaluated high burn-up conditions in LWRs and confirmed that off-centered, solid pellets operate at lower temperatures than concentric ones. Williamson et al. (2021) validated 3D FEM simulations using BISON against LWR experimental data, specifically accounting for pellet eccentricity. The validation includes integral non-hollowed LWR experiments such as the IFA-431 rod 4 (Williamson et al., 2016), which explicitly considered pellet offset, as reported by Hales et al. (2013). The results indicate that the temperature difference between concentric and off-centered pellets arises not only because concentric pellets tend to reach higher temperatures, but also because the peak temperature in off-centered pellets is shifted away from the

☆ This article is part of a special issue entitled: 'alternative fuels' published in Nuclear Engineering and Design.

* Corresponding author at: Politecnico di Milano, Department of Energy, Nuclear Engineering Division, via La Masa 34, 20156 Milano, Italy.
E-mail address: diego.jaramillo@enea.it (D. Jaramillo-Sierra).

https://doi.org/10.1016/j.nucengdes.2025.114372
Received 13 February 2025; Received in revised form 29 June 2025; Accepted 31 July 2025
Available online 7 August 2025

Nomenclature

BoL	Beginning of Life
BFC	Bottom Fuel Column
EFPD	Equivalent Full Power Day
EoL	End of Life
FEM	Finite Element Method
FPC	Fuel Performance Code
FR	Fast Reactor
HFR	High Flux Reactor
LHR	Linear Heat Rate
LWR	Light Water Reactor
MFP	Maximum Flux Plane
MOX	Mix Oxide
MTR	Material Test Reactor
PIE	Post Irradiation Examination
PuMMA	Plutonium Management for More Agility

centerline.

Maeda et al. (2011) analyzed the B14 short-term irradiation test with Am-MOX fuel, which resulted in significant fuel relocation and off-centered fuel restructuring. Building on these findings, Ozawa et al. (2021) applied a new BISON model to study pore migration and its role in fuel restructuring. However, neither study observed an increase in the maximum fuel temperature.

Further evidence involving full MOX fuel comes from Harp and Chichester (2017). In the AFC-2C experiment, the fuel reached up to 8 % burn-up, and rodlet 2CR3 exhibited off-centering. The authors suggest that this off-centering is likely due to the rodlet not being exactly centered in the capsule. Despite the off-centering, the non-hollowed fuel still reached the temperatures required for restructuring.

Novascone et al. (2018) investigated porosity migration in oxide fuels using FEM. In their validation, they observed that the central void, in addition to being off-centered, exhibited an elliptical shape, with the major axis of the ellipse oriented orthogonally to the temperature gradient.

Fewer studies have focused on hollow pellets. Harayama and Kyoya (1986) evaluated annular pellets, demonstrating that hole eccentricity shifts the maximum temperature opposite to the displacement, which increases both the peak temperature and the extent of the high-temperature region.

Studies made on annular fuel geometries include Deng and co-authors study (Deng et al., 2019) on the Internally and eXternally cooled Annular Fuel (IXAF) design (Carpenter et al., 2006) using BISON, which concluded that off-centering can significantly increase peak fuel temperatures and cladding hoop stress, factors that could jeopardize fuel integrity under both operating and transient conditions. Because the IXAF concept features both internal and external cooling as well as higher fuel thermal conductivity, its thermo-mechanical behavior cannot be assumed valid for hollow MOX pins operating in a fast neutron spectrum; it therefore remains to be established whether Deng et al.'s conclusions hold for fast reactor (FR) MOX hollow fuel.

Similarly, Blanc and co-authors (Blanc et al., 2017) simulated hollow MOX fuel using the LICOS code (Helfer et al., 2015) and identified eccentricity and hole misalignments as two of the main parameters that reduced the margin to fuel melting during early irradiation stages. Their assessment, however, was limited to beginning-of-life conditions and did not capture the overpower periods that arise later in the irradiation history, such as those experienced by the TRABANT-2/2 pin, addressed in the present work.

These findings suggest that off-centering effects should be included in safety assessments, especially for hollow fuels with low thermal conductivity and high-power density. While off-centering generally reduces pellet temperatures in solid LWRs and high-conductivity metallic fuels, the overall impact on fuel performance and safety is complex. The literature suggests that off-centering increases stress and loading asymmetry in the cladding, adversely affecting cladding integrity.

This is particularly relevant for Gen-IV designs using MOX fuel, where the presence of minor actinides and low thermal conductivities could amplify off-centering effects. Therefore, this work explicitly investigates these effects, and their implications should be incorporated into design and safety evaluation of advanced fuels, especially for hollow geometries and high-Pu content fuels.

1.1. PuMMA project and PIE observations

The EU-funded PuMMA (Plutonium Management for More Agility) project focuses on evaluating the impact of high plutonium content MOX fuels on reactor safety and performance (Chauvin et al., 2022). Recent post-irradiation examinations (PIE) of two experimental fuel pins, CAPRIX (45 % Pu) and TRABANT-2/2 (40 % Pu), revealed significant off-centering of the central hole (Fayette et al., 2022; Van Til et al., 2024; van Til et al., 2025). Although the pellets were fabricated by JRC (CAPRIX) and CEA (TRABANT-2/2) using best-practice procedures to ensure concentricity of both the central void and the pellet-to-cladding alignment, considerable eccentricities nonetheless developed during irradiation. The PIE at Maximum Flux Plane (MFP) for CAPRIX and TRABANT-2/2 are reported in Fig. 1: these results underscore the importance of modeling off-center fuel behavior to assess its impact on melting margins under normal and incidental conditions.

As part of the PuMMA effort, this work aims to model fuel behavior under eccentric conditions by employing advanced asymmetrical models. The objective is to reproduce the dynamics between temperature profiles and pore migration and to validate the results based on the PIE findings.

2. Irradiation experiments description

Table 1 summarizes the key specifications of the CAPRIX and TRABANT-2/2 irradiation experiments, which serve as the input parameters for analyzing the performance of the two fuel pins. These experiments provide valuable context for understanding the irradiation conditions, which are critical for evaluating the behavior of MOX fuel, particularly with high plutonium content, under reactor-relevant conditions.

The CAPRIX experiment was conducted in the PHENIX fast reactor, spanning from 1995 to 2006, with an equivalent full power duration of approximately 620 days (Venard and Deveaux, 2021), whereas the TRABANT-2/2 experiment – part of the Transmutation and Burning of Actinides in TRIOX series – took place in the High Flux Reactor (HFR) in Petten. This experiment aimed to assess the feasibility of burning plutonium and transmuting minor actinides in fast breeder reactors. The

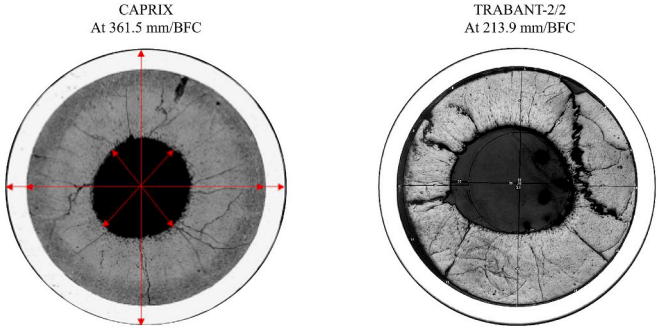

Fig. 1. Post-irradiation examination of CAPRIX (left) and TRABANT-2/2 (right) at MFP.

Table 1
Irradiation experiments specifications.

Pin specifications	CAPRIX	TRABANT-2/2
Reactor	PHENIX (FR)	HFR (MTR)
Equivalent irradiation time (days)	620.4	74.1
Max. LHR (W/cm)	354	465
Max. Cladding temperature (K)	750	839
Fuel type	MOX	MOX
Manufacturer	JRC	CEA
Active length (mm)	850	340
Fuel central hole diameter (mm)	2.0	2.39
Fuel pellet diameter (mm)	5.42	5.426
Initial gap width (mm)	0.115	0.112
Total porosity (%)	5.47	6.5
Oxygen to metal ratio	2.00	1.995
Heavy metal composition	U: 55 % Pu: 45 %	U: 60 % Pu: 40 %
Cladding material	AIM1	15–15 Ti SS
Cladding outer diameter (mm)	6.55	6.55
Cladding inner diameter (mm)	5.65	5.65
Filler gas pressure (bar)	1	1
Filler gas composition	He: 95 %, N_2: 5 %	He: 100 %

irradiation was conducted over multiple cycles between 2001 and 2005 but was ultimately discontinued due to significant fuel axial displacement observed through neutron-radiography (Van Til et al., 2021). The nominal cladding temperature and linear heat rate (LHR) at the peak power position are illustrated in Fig. 2 for both the considered experiments.

3. Model description

This work builds on the research by Barani and co-authors (Barani et al., 2022), who developed an engineering-scale model for porosity migration using the open-source C++ library MFEM (Anderson et al., 2021). MFEM serves as the foundation for efficiently solving partial differential equations via the finite element method, supporting arbitrary high-order finite elements, scalable parallelization, and compatibility with external tools such as GMSH (Geuzaine and Remacle, 2009) and ParaView (Ahrens et al., 2005). These tools were employed throughout this study. The model aims to couple the heat diffusion equation with pore advection into a solvable system, as described below:

$$\rho c_p \frac{\partial T}{\partial x} - \nabla \bullet [k(T,p)\nabla T] - q_v \frac{1-p}{1-p_0} = 0 \tag{1}$$

$$\frac{\partial p}{\partial t} + \nabla \bullet [\mathbf{v}(T)p] = 0 \tag{2}$$

In this set of equations, the terms are defined as follows:

- ρ ($kg \cdot m^{-3}$): fuel density
- c_p ($J \cdot kg^{-1} \cdot K^{-1}$): heat capacity
- T (K): temperature
- $q_v (W \bullet m^{-3})$: volumetric heat source
- $p_0, p(-)$: initial and current porosity
- $k(T,p)(W \bullet m^{-1} \bullet K^{-1})$: thermal conductivity
- $\mathbf{v}(T)(m \bullet s^{-1})$: pore velocity

In this work, the thermal conductivity $k(T,p)$ is described using the Kato (KATO et al., 2011) formulation with a porosity correction based on the Maxwell-Eucken model (Eucken, 1940):

$$k(T) = \frac{1}{A + BT} + \frac{C}{T^{\frac{5}{2}}} \exp\left(-\frac{D}{T}\right) \tag{3}$$

with the coefficients defined as:

- $A = (2.713x + 3.583 \times 10^{-1} \times z_1 + 1.595 \times 10^{-2})$
- $B = (-2.625x + 2.493) \times 10^{-4}$
- $C = 1.541 \times 10^{11}$
- $D = 1.522 \times 10^{4}$

The effective thermal conductivity, corrected for porosity, is given by:

$$k(T,p) = k(T)\frac{k_{He} + 2k(T) - 2p(k(T) - k_{He})}{k_{He} + 2k(T) + p(k(T) - k_{He})} \tag{4}$$

The formulation captures two dominant conduction mechanisms: a hyperbolic term accounting for the lattice conduction by phonons and an Arrhenius-type term associated with electron-vacancy pair mobility. The correlation includes the effects of stoichiometry (x) and americium content (z_1), while neglecting corrections for neptunium. The porosity is treated by assuming that all pores are filled with helium, using a constant thermal conductivity k_{He} equal to 0.69 $W \cdot m^{-1} \cdot K^{-1}$.

Various correlations for pore velocity are available in literature, considering different physical dependencies. In this study, the expression proposed by Sens (Sens, 1972) is adopted:

$$|\boldsymbol{v}| = c_0(c_1 + c_2 T + c_3 T^2 + c_4 T^3)\Delta H_s P_{0,s} \exp\left(-\frac{\Delta H_s}{RT}\right) T^{-2.5} |\nabla T| \tag{5}$$

Here c_0, c_1, c_2, c_3 and c_4 are constants, $\Delta H_s (Jmol^{-1})$ is the heat of vaporization, $P_{0,s}$ is a characteristic material parameter and $R(Jmol^{-1}K^{-1})$ is the universal gas constant.

The system of equations is solved using the Streamline Upwind stabilization technique for the pore advection equation, to limit the spatial oscillations in the solution of this advection-dominated PDE. However, the presence of non-uniform source terms and asymmetries can lead to an excessive introduction of diffusivity by this stabilization approach.

As discussed in detail in section 6.3, the present MFEM model includes several simplifications that define its scope and limitations: It uses a 2-D representation with assumed symmetry and does not account for any axial coupling. Solid mechanics effects, such as elastic or plastic

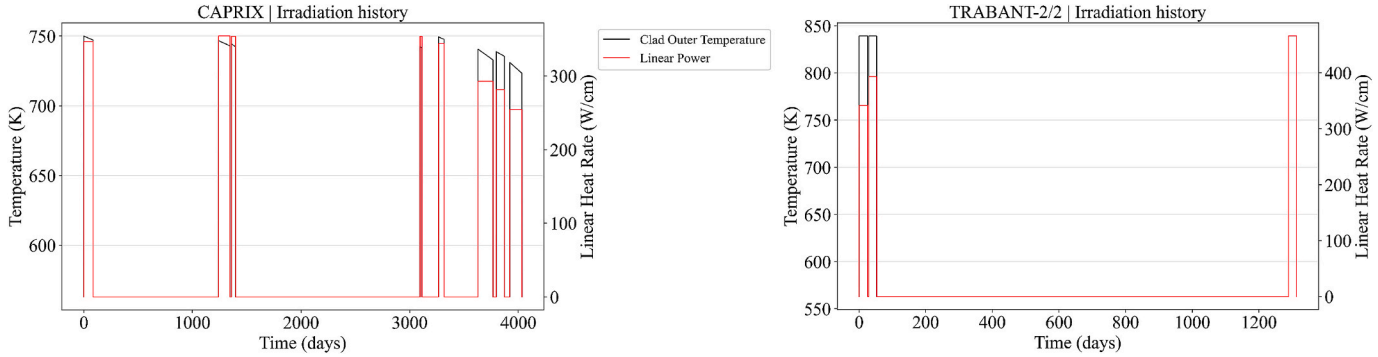

Fig. 2. CAPRIX (left) and TRBANT-2/2 (right) Cladding nominal temperature and LHR at the peak power position.

deformation and cladding creep are not explicitly modelled. The fuel thermal conductivity is kept constant, not accounting explicitly for burn-up degradation. Other effects, including redistribution, oxygen-to-metal (O/M) ratio changes are also neglected. Finally, boundary cladding temperatures are taken directly from the fuel performance codes, without experimentally measured angular data.

3.1. Mesh generation

The displacement of the pellet within the cladding can be described as in Fig. 3. It is possible to derive the analytical solution for an independent displacement in the x and y directions. However, a simpler and equivalent solution is to change the reference coordinate system, through rotation, forcing it to overlap with a new x axis. In this way, after rotating the reference frame, it is possible to represent any two-dimensional displacement in an equivalent new x-directional displacement in the new reference system. This approach simplifies the number of case studies relevant to consider, allowing for the assumption of symmetry along the new x-axis for all possible displacements. Therefore, it is possible to consider a half-pellet domain, reducing by half the number of mesh points and the overall computational cost.

All the meshes used in this work are produced using the open-source code GMSH, starting with a simple uniform mesh, the following optimization process led to the reference meshes used in this work:

1. Identification of the regions of big discontinuities (pore velocity and porosity).
2. Mesh refinement in the identified regions.
3. Verification of the quality of the mesh by comparing the aspect ratio of the elements, the number of elements and their size.
4. Iterate the previous steps until the mesh is satisfactory.

The reference mesh for CAPRIX is presented in Fig. 4 (left). In the outer region the element size is set to be equal to half outer arc, while in the innermost part of the pellet it is fixed to one twentieth of inner arc. The transitions between elements are imposed using a radial threshold field, up to a radius of expected porosity discontinuity the element sizes are set to minimum, for increasing radius the size increases gradually up to the maximum size at the outermost boundary (fuel pellet surface).

A second version of this mesh is made for TRABANT-2/2, presented in Fig. 4 (right) as higher linear heat rates produce significant pore velocity discontinuities. Therefore, the resulting mesh extends the minimum size band to the region where the maximum pore velocity is expected. The results improve significantly and even if computational cost increased, the simulation times remain reasonable for the scope of this work.

The Table 2 provides a detailed comparison of mesh statistics for the two cases, including key metrics such as element counts and quality indicators.

3.2. Boundary conditions

The MFEM model requires data for the fuel surface temperatures, which are obtained from the fuel performance calculations conducted as part of the PuMMA benchmark Phase I (Jaramillo-Sierra et al., 2025). The reference results (centered pellet) for TRANSURANUS (Magni et al., 2021) and GERMINAL (Lainet et al., 2019) codes are reported in Figs. 5 and 6.

It is important to note that, although both codes were supplied with harmonized irradiation inputs, including irradiation history, cladding temperature, fuel composition, and geometry, the predicted outer fuel temperatures differ significantly. These discrepancies derive from differences in material property correlations and in the treatment of key thermal–mechanical phenomena such as gap conductance, fuel relocation, and Joint-Oxide-Gaine formation.

These divergences were already evident in the blind phase of the PuMMA benchmark and are described in detail in its corresponding publication, which includes a detailed description of the models and material properties used by each code (Jaramillo-Sierra et al., 2025). The most relevant differences and their implications for MFEM simulation outcomes are further analyzed in Section 6.2.

To consider a non-homogeneous angular boundary condition, the coordinate reference system is fixed at the center of the fuel pellet where the distance of the displacement is ε and the angle considered is θ, as shown in Fig. 7. The gap distance g between the fuel outer radius r_f and the cladding inner radius r_c is then a function of the displacement and the angle considered g (ε, θ). Following simple geometry reasoning it is possible to derive the analytical function as follows:

$$g(\varepsilon,\theta) = \sqrt{r_c^2 - \varepsilon^2 \sin^2(\theta)} - \varepsilon\cos(\theta) - r_f \tag{6}$$

To calculate the pellet surface temperature as function of the angle, a gap size sensitivity is performed in for both the codes involved. The gap size is calculated for 11 equally spaced angles from 0° to 180°, and the corresponding values are implemented in the codes by increasing the inner cladding radius.

The initial ramp to achieve the nominal LHR takes one hour. At this time, the angular temperature distribution determined by gap size sensitivity is analyzed while the gap remains open. Fig. 8 illustrates the outer fuel temperatures as a function of angle. It is noteworthy that the temperature variation between the two codes reaches approximately 500 °C, primarily due to the different fuel radial relocation models employed by each code.

According to the GERMINAL results, the gap between the fuel and cladding closes during the first cycle. After gap closure, the angular temperatures shown in Fig. 12 become uniform, aligning with the reference (centered) case. In contrast, the TRANSURANUS simulations do not predict gap closure, implying that the angular temperature distribution applied in the MFEM model will maintain the same shape as depicted in Fig. 8 throughout the entire irradiation.

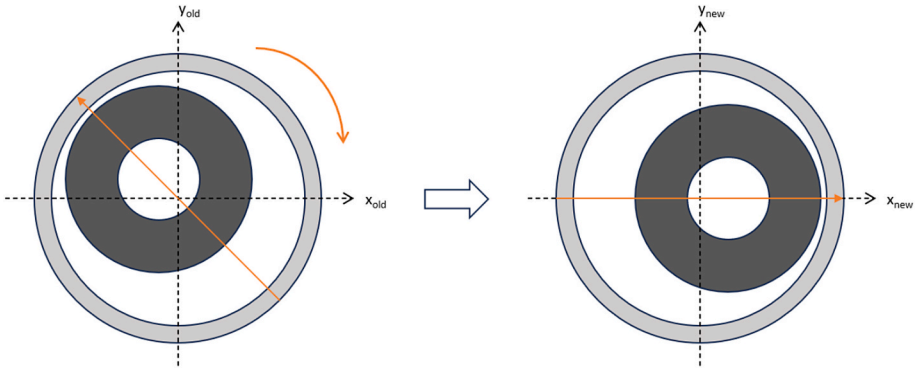

Fig. 3. Scheme of directional displacement equivalency.

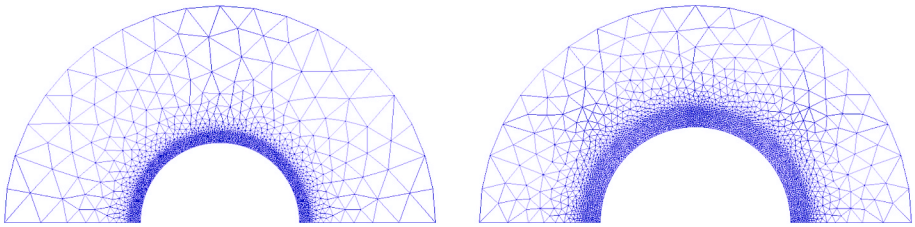

Fig. 4. Mesh for CAPRIX (left) and TRABANT-2/2 (right) simulations.

Table 2
Comparison of mesh statistics for CAPRIX and TRABANT-2/2 cases.

Property	CAPRIX	TRABANT-2/2
Nodes	2272	2923
Triangles	4328	5635
SIGN[1]	0.9443 (0.7416 → 1)	0.9445 (0.717 → 1)
Gamma[2]	0.9347 (0.657 → 1)	0.9348 (0.623 → 1)
SIGE[3]	0.9761 (0.8416 → 1)	0.9761 (0.8215 → 1)

[1]SICN: signed inverse condition number.
[2]Gamma: inscribed radius / circumscribed radius.
[3]SIGE: signed inverse error on the gradient of FE solution.

4. MFEM calculations results

This section presents and analyzes the outputs of the MFEM simulations to evaluate the impact of off-centering on pore migration under boundary conditions from two reference FPCs: GERMINAL and TRANSURANUS. The analysis focuses on directional pore migration and temperature distributions. The two times considered were intentionally selected: the 1-hour mark (BoL) corresponds to the peak of the linear heat rate ramp, before gap closure occurs, and represents the most conservative condition for assessing the melting margin, since GERMINAL predicts the highest fuel temperatures at this stage. The EOL, by contrast, captures the cumulative effects of porosity migration and is therefore relevant for comparing the final state between both cases and with experimental observations.

Additionally, two parametric cases are detailed in the appendix: one exploring the effect of a 10 % variation in the thermal conductivity within the MFEM model, and the other examining the behavior under central hole misalignment. These cases provide further insights into the robustness of the model and its response to modeling and manufacturing uncertainties.

4.1. CAPRIX

4.1.1. Centered case

According to the reference fuel performance calculations, the

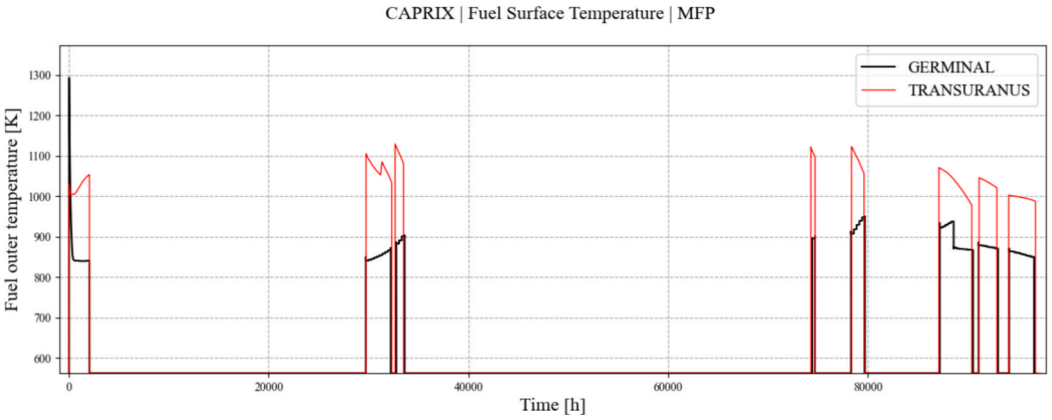

Fig. 5. CAPRIX Fuel surface temperatures at MFP: reference simulation.

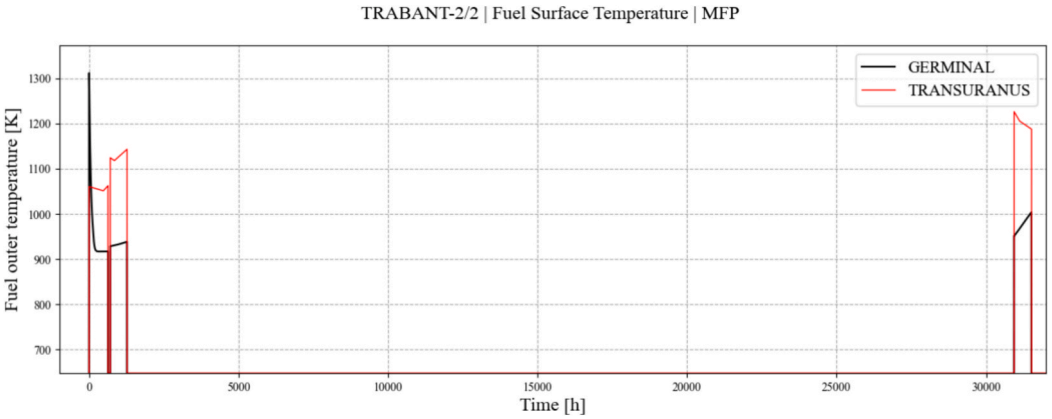

Fig. 6. TRABANT-2/2 Fuel surface temperatures at MFP: reference simulation.

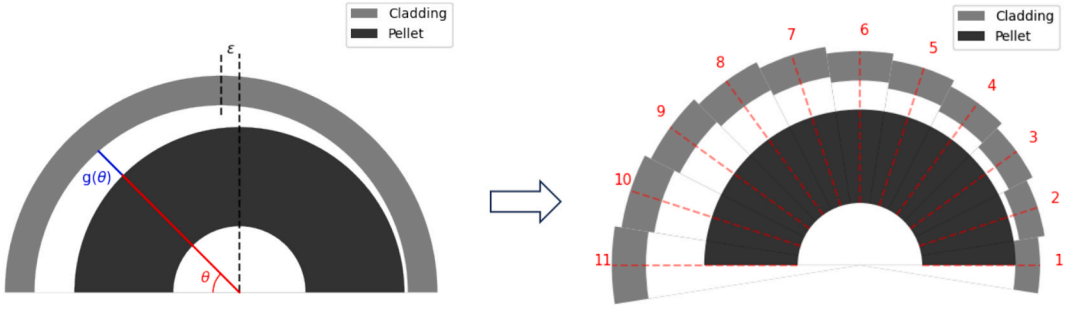

Fig. 7. Schemes for directional displacement gap size (left) and sensitivity (right).

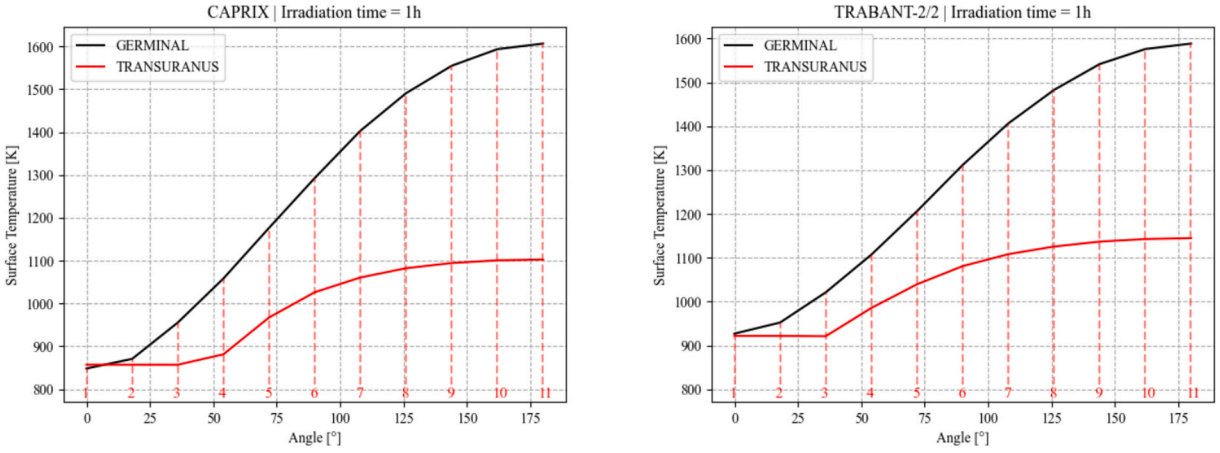

Fig. 8. Angular temperature profile for CAPRIX (left) and TRABANT-2/2 (right).

maximum fuel temperature for GERMINAL was reached after 1 h of irradiation. As anticipated, higher temperatures led to increased pore velocities, resulting in more pronounced porosity migration, as illustrated in Fig. 9. In contrast, for MFEM-TRANSURANUS (MFEM-TU), the imposed boundary conditions resulted in both lower temperatures and reduced pore migration.

4.1.2. *Off-centered case*

In the off-centered case, the MFEM model predicts higher temperatures on one side of the pellet after 1 h of irradiation under both boundary conditions, with MFEM-GERMINAL (MFEM-GE) exhibiting the highest temperatures. The temperature distribution is highly sensitive to the boundary conditions; consequently, at the End of Life (EoL), the MFEM-TU model presents a higher temperature profile. Notably, in the MFEM-GE simulation, the region of higher temperature shifts to the opposite side. This behavior can be attributed primarily to the gap closure predicted by GERMINAL during the first cycle. From a thermal perspective, the gap closure enhances its conductance, leading to a global reduction in temperatures. However, since anisotropic pore migration occurs prior to gap closure, the homogenization of surface temperatures results in a higher temperature profile in the non-restructured region. At EoL, both simulations demonstrate significant directional pore migration, with local porosity values reaching 100 % for MFEM-GE and 60 % for MFEM-TU. All these trends are illustrated in Fig. 10.

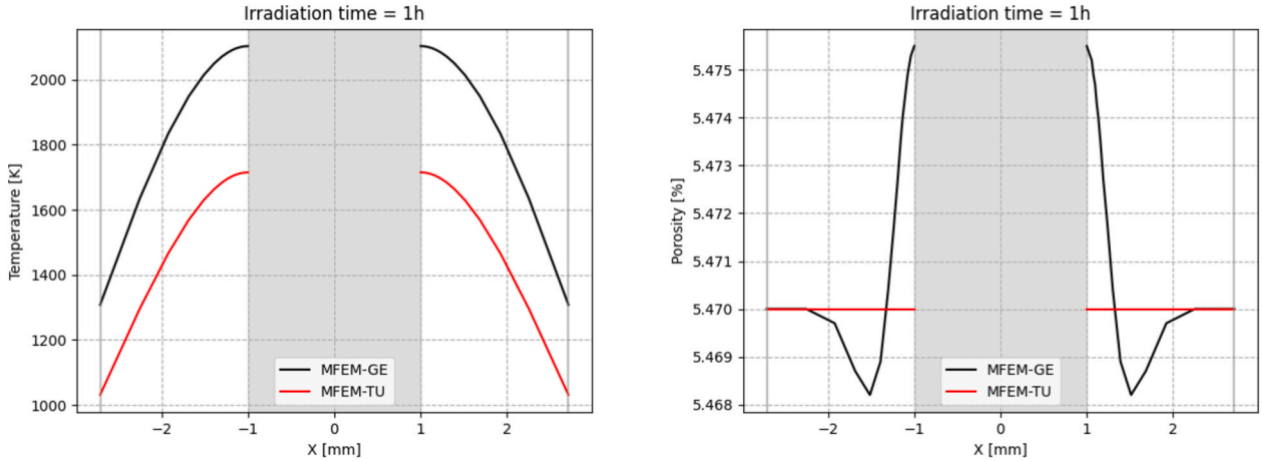

Fig. 9. CAPRIX Centered case temperature, and porosity at 1 h.

4.2. TRABANT-2/2

4.2.1. Centered case

Similarly to the CAPRIX case, the centered pellet reference case for TRABANT-2/2 exhibited higher temperatures for MFEM-GE, as expected, after 1 h of irradiation, as shown in Fig. 11. In contrast, MFEM-TU resulted in lower initial porosity migration, consistent with its corresponding temperature profile.

4.2.2. Off-centered case

In the off-centered case, the MFEM model at one hour of irradiation shows both higher temperatures on one side of the pellet and anisotropic pore migration for MFEM-GE. As expected from previous analyses, MFEM-GE initially produces higher temperatures, consistent with the imposed boundary conditions. However, this trend does not persist throughout the entire irradiation period. Since GERMINAL predicts gap closure early in the first irradiation cycle, the temperature profile becomes less sensitive to conditions during the third cycle, when the pin undergoes over-power conditions. Consequently, at EoL, MFEM-TU exhibits a more pronounced final porosity distribution, along with a higher temperature profile. Notably, the behavior observed in the MFEM-GE simulation for the CAPRIX pin is replicated here: after gap closure in an already directionally restructured pellet, the region of higher temperatures shifts to the opposite side. All these results are illustrated in Fig. 12.

5. Comparison against PIE

Based on the PIEs of PUMMA, a semi-quantitative validation of the MFEM model can be established. This semi-quantitative approach is chosen to provide a balanced evaluation of the phenomena, recognizing both the strengths and limitations of the model. Figs. 13 and 14 present a direct comparison between the model's predictions and the behavior observed in the CAPRIX and TRABANT-2/2 fuels, respectively.

The primary validation parameter is the directional enlargement of the central hole, consistently observed in all off-centered case studies. This enlargement is reproduced with reasonable accuracy by the MFEM-GE model in the CAPRIX case and by the MFEM-TU model in the TRABANT-2/2 case. Table 3 provides a direct comparison of the central hole enlargement across the studied cases.

These geometrical results should be interpreted considering the model limitations, particularly its inability to fully replicate the permanent and non-elastic deformation that the fuel pellet undergoes during normal irradiation. Such deformations arise from complex interactions between thermal, mechanical, and irradiation-induced phenomena, which are not captured within the assumptions and formulations of the MFEM model.

While validating the temperature profile directly is not feasible, the porosity reduction serves as a useful proxy for assessing the model ability to simulate this quantity. For CAPRIX, the PIE data show a porosity reduction that aligns well with the results of both MFEM simulations. However, this agreement is not observed in the TRABANT-2/2 case, where experimental images do not exhibit comparable behavior.

6. Discussion and safety implications

This section discusses the impact of off-centering effects on fuel safety, focusing on the reduction of the margin to melt and its stochastic relevance, as well as the spread introduced by different FPCs and the strengths and limitations of the proposed modeling approach.

6.1. Margin to melt reduction and stochastic relevance

This work successfully replicates the anisotropic enlargement of the central hole observed in PuMMA experiments and provides a deeper understanding of the dynamics leading to increased temperatures. As

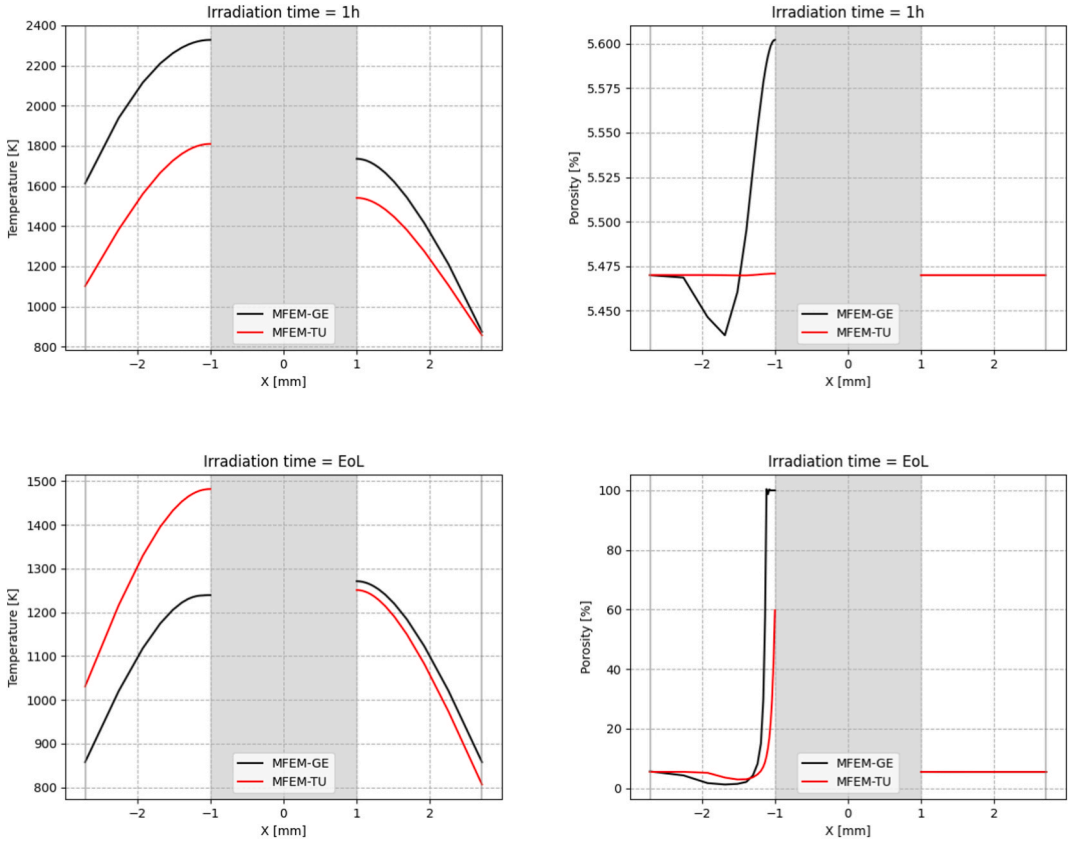

Fig. 10. CAPRIX Off-centered case temperature and porosity at 1 h and EoL.

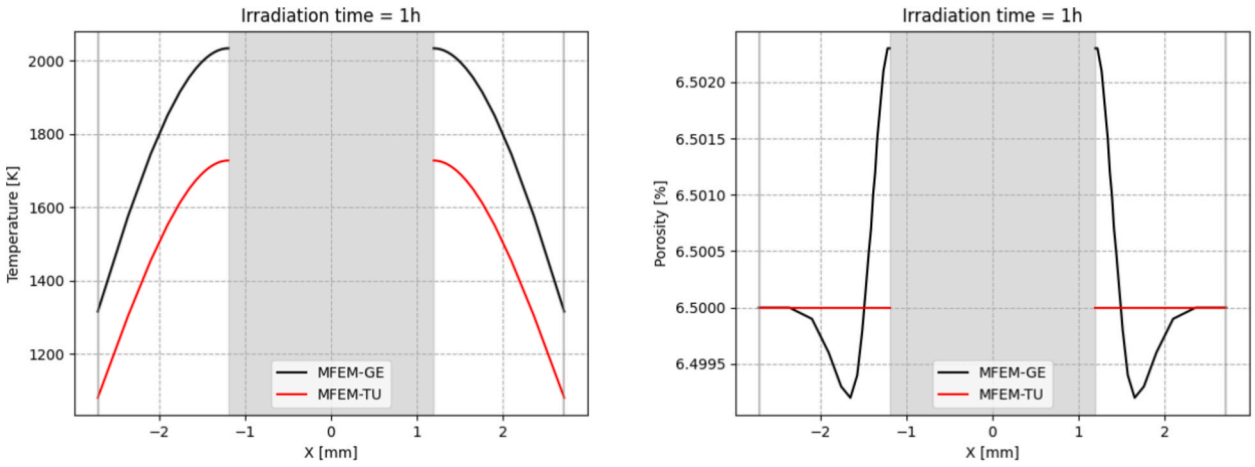

Fig. 11. TRABANT-2/2 Centered case temperature, and porosity at 1 h.

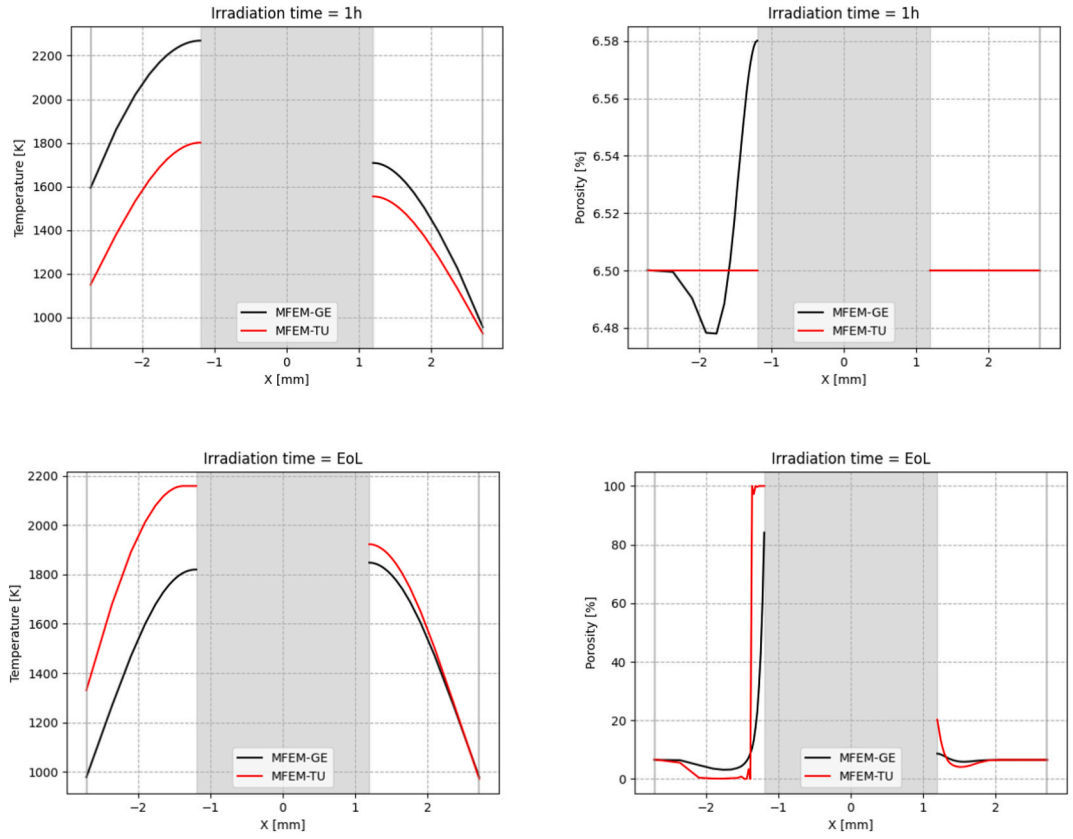

Fig. 12. TRABANT-2/2 Off-centered case temperature, and porosity at 1 h and EoL.

noted in the introduction, off-centering and hole misalignments were identified as critical factors reducing the margin to melt during early irradiation stages (Blanc et al., 2017). Quantifying and understanding these dynamics are essential, as the margin to melt (the temperature difference between the fuel and its melting point) is a critical parameter for the safe operation of nuclear fuel, particularly for fuels with lower thermal conductivity.

Fig. 15 illustrates how off-centering leads to localized temperature increases across all simulations, with the highest temperatures observed opposite the fuel-cladding contact point. This effect is particularly pronounced in hollow fuel pellets, such as those studied in the CAPRIX and TRABANT-2/2 experiments. The temperature increase ($\Delta T_{\text{off-centering}}$) is substantial, ranging from 73–95 °C in MFEM-TU and 224–235 °C in MFEM-GE. Such increases elevate the risk of fuel melting during operational transients or unanticipated power spikes. In fact, these effects are not limited to the first stages or the irradiation; as shown in the TRABANT-2/2 case, they can significantly impact fuel behavior throughout subsequent cycles.

The exact causes of off-centering are challenging to identify and may be influenced by factors such as fuel shuffling between cycles, the roughness of MOX pellets, or misalignment during the mounting phase of the fuel pin. Given the small dimensions involved, assembly tolerances could also contribute to off-centering. While directly determining the cause is challenging and the phenomenon may appear stochastic, its apparent randomness arises from insufficient input data and incomplete boundary conditions necessary for accurate simulation and prediction. It

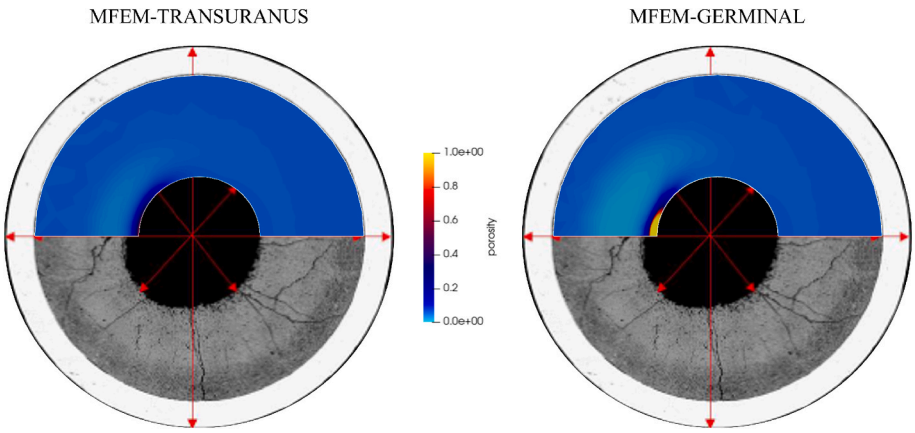

Fig. 13. CAPRIX comparison against PIE: MFEM-TU (left) and MFEM-GE (right).

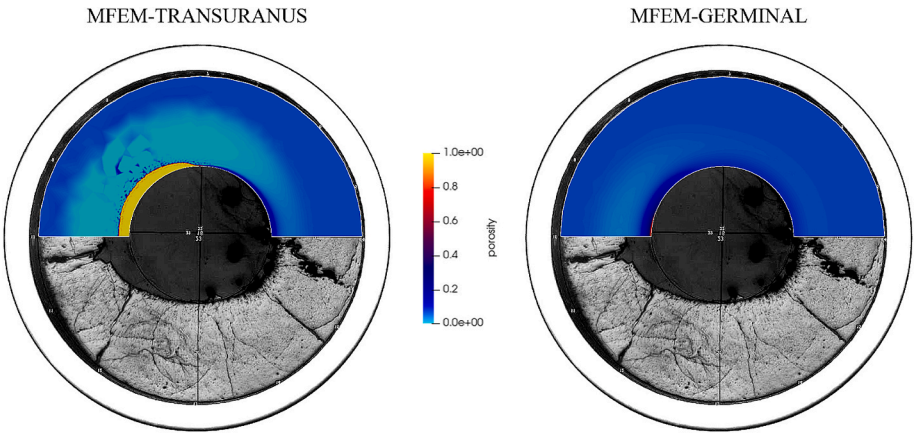

Fig. 14. TRABANT-2/2 comparison against PIE: MFEM-TU (left) and MFEM-GE (right).

Table 3
Comparison of central hole diameters (mm) for CAPRIX and TRABANT-2/2 cases.

	CAPRIX		TRABANT-2/2	
	Min	Max	Min	Max
MFEM-GERMINAL	2.00	2.139	2.39	2.428
MFEM-TRANSURANUS	2.00	2.01	2.406	2.569
PIE	2.250	2.460	2.513	2.841

is important to emphasize that asymmetric neutron flux profiles are very unlikely to be the main driver of the observed void asymmetry, as this behavior is observed in fuels irradiated in both FRs and MTRs and is also supported by PIE reports (van Til et al., 2025).

6.2. FPCs models and temperature spread

The results highlight the sensitivity of the MFEM model to the boundary conditions imposed by different FPCs. The decision to include two different FPCs in the analysis derives from the significant spread in results observed during the initial phase of the PuMMA benchmark exercise.

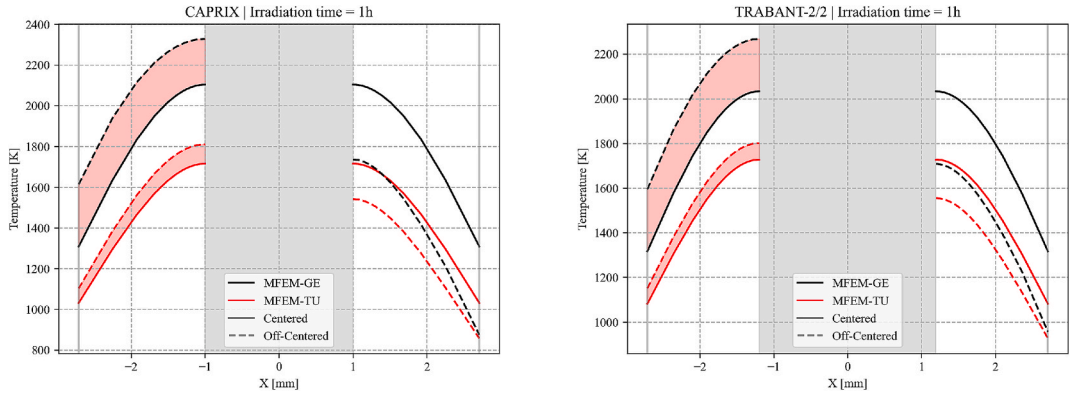

Fig. 15. Temperature increases in CAPRIX (left) and TRABANT-2/2 at 1 h.

The variability in the FPCs output originates from several factors, including user-defined reference models, correlations specific to each code, and differences in operating principles, underlying physical models, and the emphasis placed on competing phenomena. This divergence is evident when comparing the behavior of the GERMINAL and TRANSURANUS.

In the case of CAPRIX, GERMINAL predicts a rapid temperature increase, with the fuel surface reaching 1300 K within the first hour of irradiation. This leads to early gap closure after the initial 20 days of the cycle, reducing surface temperatures to approximately 900 K for the remainder of the cycle. On the contrary, TRANSURANUS does not exhibit such a temperature spike. Instead, it predicts a consistent surface temperature of 1000 K throughout the first cycle, delaying gap closure until the fifth cycle.

Key differences between the codes can be attributed to their respective fuel fragment radial relocation and gap conductance models. TRANSURANUS employs a straightforward relocation model that bases changes on the initial gap size. In contrast, GERMINAL's model accounts for the complete evolution of the free volumes created by cracking at the beginning of life. Its empirical formulation includes a dependence of the fragment relocation on the thermal gradient within the pellet, which is indeed the main driver of gap closure in the fuel (Lainet et al., 2019).

After GERMINAL gap closure, the two codes diverge further. GERMINAL predicts lower overall temperatures due to enhanced gap conductivity from fuel-cladding contact, while TRANSURANUS predicts higher temperatures, not only because it assumes an open gap but also due to elevated FGR, which degrades gap conductance. These differences critically influence analyses of pore migration, especially during scenarios of high LHR.

For CAPRIX, GERMINAL predicts conservatively high temperatures, which aligns with high LHR at the BoL (time = 1 h). However, in cases like TRABANT-2/2, where the highest LHR occurs during the third cycle, early gap closure predicted by GERMINAL can underestimate temperatures. PIEs corroborate these findings in both CAPRIX and TRABANT-2/2 cases.

6.3. Strengths and limitations of the proposed method

The results demonstrate that the proposed model effectively replicates non-axially symmetric pore migration, establishing itself as a valuable tool for interpreting PuMMA PIEs and for semi-quantitatively predicting the effects of off-centering phenomena. However, the model accuracy is constrained by the limited physics included in the description (i.e., no mechanics, redistribution of constituents or isotopic evolution).

Key limitations include neglecting significant long-term irradiation effects such as thermal conductivity degradation due to burn-up, and power distribution changes induced by plutonium and americium redistribution. While incorporating thermal–mechanical coupling and cladding behavior could significantly enhance the model predictive capabilities, it would also increase its complexity and computational demands.

Accurate predictions are further complicated by the conditions under which the fuel pins are irradiated. The absence or non-availability of angular cladding temperature measurements makes it challenging to define precise boundary conditions. Additionally, irradiation in a thermal/epithermal reactor (e.g., HFR) can significantly impact power deposition within the material, further complicating the analysis. Factors such as the decreasing effectiveness of the neutron shield and the evolving neutron spectrum can alter the fuel's effective cross-sections over time. In the TRABANT-2/2 case, PIE reveals that the axial profile of central hole enlargement is not directionally uniform but exhibits an oscillatory pattern. This suggests that the phenomenon may be influenced by evolving irradiation conditions and underscores the need for angular data to refine the model and improve its reliability.

7. Conclusion

This work investigates the effects of pellet off-centering on the behavior of hollow MOX fuel with high plutonium content, using a FEM model implemented through the MFEM library. The model couples heat conduction with pore migration equations to simulate anisotropic porosity evolution and temperature distributions under fast reactor irradiation conditions. The analysis focuses on two experimental fuel pins from the PuMMA project, CAPRIX and TRABANT-2/2, both of which exhibited significant eccentricity in PIE. The simulations successfully reproduce these conditions and compare results with PIE findings to assess the impact of eccentricity on melting margins and fuel behavior.

The key findings of this work include:

1. **Off-centering effects on temperature distribution**: Pellet eccentricity induces localized temperature peaks in hollow pellets, reducing the margin to melting under both normal and transient operational conditions. In some cases, this effect leads to temperature increases of up to 235 °C. These results highlight the necessity of considering eccentricity in fuel performance models, especially for reactors operating at high temperatures and LHRs.
2. **Directional pore migration**: The model successfully replicates the asymmetric porosity observed in PIE, particularly in the enlargement of the central hole. While the MFEM-GERMINAL model aligns well with CAPRIX PIE results, the MFEM-TRANSURANUS model captures better the behavior observed in TRABANT-2/2, emphasizing the strong dependency on FPC boundary conditions.
3. **Sensitivity to FPC modeling approaches**: Differences in fuel performance modeling significantly influence the predicted temperature distribution and porosity migration. The analysis highlights the variability in fuel-cladding gap dynamics, gap conductance and fuel fragmentation models, which lead to divergent predictions of gap closure and subsequent thermal conditions. This highlights the need for standardized approaches to fuel modeling to reduce uncertainties in safety assessments.
4. **Safety implications**: Off-centering leads to significantly temperature increases and directional porosity migration, potentially impacting the integrity of the fuel and cladding. Given the uncertain origin of pellet eccentricity, possibly caused by assembly tolerances or pellet roughness, these phenomena should be systematically integrated into safety evaluations and design optimization of Gen-IV reactors. This is particularly important for reactors featuring hollow ceramic fuels or other designs with high-power densities, elevated temperatures, and low thermal conductivities.

7.1. Future perspectives

While this work advances the understanding of off-centering effects of off-centering in hollow MOX fuels, it also highlights areas requiring further investigation:

- **Incorporation of thermal–mechanical coupling**: Future models should integrate mechanical behavior, including stress–strain interactions, pellet-cladding mechanical contact, and fuel cracking, to improve predictive capabilities.
- **Evolution of fuel properties over irradiation**: The current model does not capture phenomena such as fuel redistribution and thermal conductivity degradation over extended burn-up periods. Incorporating in the model the redistribution of plutonium, americium, and oxygen would improve the accuracy of thermal and porosity predictions. These elements influence local heat generation and fuel restructuring, making their inclusion essential for a more comprehensive assessment of fuel behavior under irradiation.

- **Experimental validation**: The current validation is limited by the lack of direct measurements of angular cladding temperature, restricting the ability to fully assess the model's predictive accuracy. Future experimental campaigns should include dedicated separate-effect tests, as well as an integral validation of the complete pore migration model. These efforts should incorporate targeted diagnostics to capture non-axially symmetric temperature and porosity distributions, providing critical data for refining computational models.

By expanding the current understanding of eccentricity-induced effects, this research contributes to improving the safety and design of hollow MOX fuels, particularly under high temperatures and LHRs in next-generation nuclear reactors.

Declaration of Generative AI and AI-assisted technologies in the writing process

During the preparation of this work the author(s) used AI-assisted technologies to improve readability and language. After using this tool/service, the author(s) reviewed and edited the content as needed and take(s) full responsibility for the content of the publication.

CRediT authorship contribution statement

D. Jaramillo-Sierra: Writing – original draft, Visualization, Validation, Methodology, Investigation, Formal analysis, Data curation. **V. Blanc:** Writing – review & editing, Validation, Supervision, Resources, Methodology, Investigation, Conceptualization. **T. Barani:** Writing – review & editing, Supervision, Software, Resources, Conceptualization. **A. Cammi:** Writing – review & editing, Supervision, Project administration, Funding acquisition. **A. Del Nevo:** Writing – review & editing, Supervision, Project administration, Funding acquisition.

Declaration of competing interest

The authors declare that they have no known competing financial interests or personal relationships that could have appeared to influence the work reported in this paper.

Acknowledgements

We gratefully acknowledge Nathalie Chauvin, whose support made this work possible.

This work has received funding from the European Union's Horizon 2020 research and innovation program through the PuMMA Project under grant agreement No 945022.

Appendix:. Parametric analysis on thermal conductivity and hole misalignment

Understanding the sensitivity of the model to key parameters such as thermal conductivity and hole misalignment is essential for evaluating its robustness and predictive accuracy. These parameters significantly impact the temperature distribution and the evolution of the central hole, both of which are critical for assessing the safety margins of high-Pu content fuels. This appendix examines the model's dependence on variations in thermal conductivity and its ability to replicate off-centering effects when accounting for initial hole misalignment.

Parametric analysis on thermal conductivity

The parametric analysis on thermal conductivity was performed using GERMINAL boundary conditions for the TRABANT-2/2 simulation. The variation range was defined as ±10 % relative to the Kato formulation (KATO et al., 2011), following the uncertainties outlined in Magni's study (Magni et al., 2020).

The results for EoL porosity are presented in Fig. 16. As expected, the model demonstrates a direct dependence on thermal conductivity, with a maximum temperature increase of 70 °C observed compared to the reference simulation. These results underscore that neglecting thermal conductivity degradation significantly limits the directional pore migration.

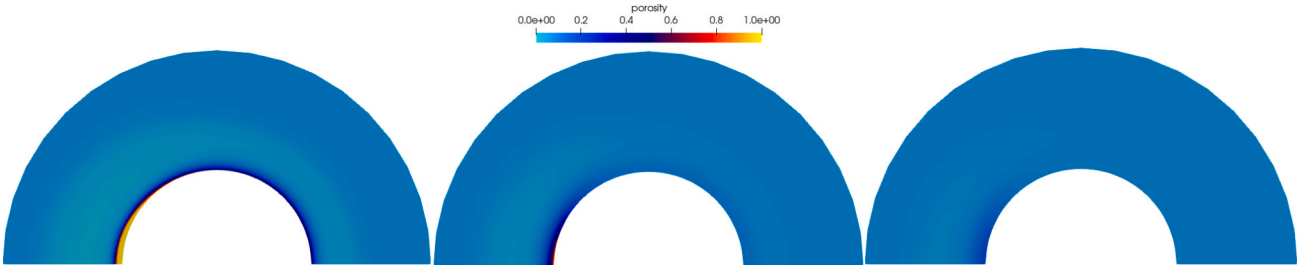

Fig. 16. TRABANT-2/2 MFEM-GE parametric results on thermal conductivity: −10 % (left), reference (center) and + 10 % (right).

Parametric analysis on central hole misalignment

Tolerances in the central hole position during MOX fuel fabrication can result in eccentric effects. To evaluate this, a significant central hole misalignment was considered by producing a new mesh with a 10 % displacement of the hole, maintaining the same quality approach as previously described. The simulation used the centered boundary conditions from the CAPRIX study with GERMINAL.

Consistent with the results from pellet off-centering, deviations from symmetric conditions (characteristic of hollow pellets) produced significant localized temperature increases, with peaks up to 150 °C. The corresponding temperature and pore migration results are shown in Fig. 17.

These findings highlight the importance of considering geometric deviations such as hole misalignment when modeling fuel behavior, as they can critically impact localized temperatures and pore migration, thereby affecting overall fuel performance and safety margins.

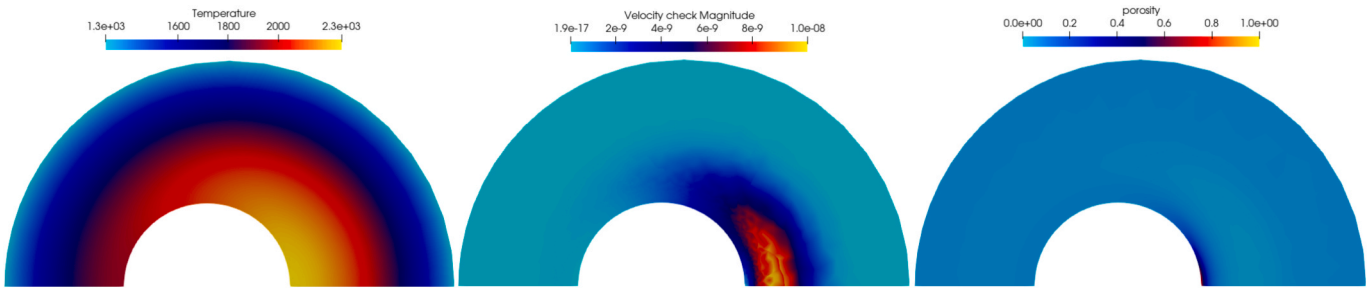

Fig. 17. CAPRIX MFEM-GE results on hole misalignment: Temperature (left), pore velocity (center) at 1 h and porosity (left) at EoL.

Data availability

Data will be made available on request.

References

Ahrens, J., Geveci, B., Law, C., 2005. ParaView: an end-user tool for large-data visualization. Visualization Handbook 717–731. https://doi.org/10.1016/B978-012387582-2/50038-1.

Anderson, R., Andrej, J., Barker, A., Bramwell, J., Camier, J.S., Cerveny, J., Dobrev, V., Dudouit, Y., Fisher, A., Kolev, T., Pazner, W., Stowell, M., Tomov, V., Akkerman, I., Dahm, J., Medina, D., Zampini, S., 2021. MFEM: a modular finite element methods library. Comput. Math. Appl. 81, 42–74. https://doi.org/10.1016/J.CAMWA.2020.06.009.

Barani, T., Ramière, I., Michel, B., 2022. Analysis of fabrication and crack-induced porosity migration in mixed oxide fuels for sodium fast reactors by the finite element method. J. Nucl. Mater. 558, 153341. https://doi.org/10.1016/J.JNUCMAT.2021.153341.

Blanc, V., Dupont, V., Beck, T., Lambert, T., Thebaud, E., Charollais, F., Pelletier, M., Bouloré, A., Dumas, J. C., Michel, B., Lainet, M., 2017. IAEA-CN-245-333 fuel melting margin assessment of fast reactor oxide fuel pin using a statistical approach.

Carpenter, D., Feinroth, H., Feng, D., Hao, B., Hejzlar, P., Kazimi, M. S., Electric, W., Kohse, C. G., Lahoda, E. J., Lee, W.-J., Mazzoccoli, J., Morra, P., Salvatore, M., Ostrovsky, Y., Russo, D. O., Otsuka, Y., Saha, P., De, F. A., Shwageraus, E., … Yuan, Y., 2006. Nuclear fuel cycle technology and policy program High Performance Fuel Design for Next Generation PWRs: Final Report. http://web.mit.edu/canes/.

Chauvin, N., Álvarez-Velarde, F., Blanc, V., Hozer, Z., Van Til, S., Boboridis, K., Maher, C., & Kampata, N. B. (2022). Presentation of the new european project PuMMA devoted to plutonium management in the whole fuel cycle.

Cunningham, M. E., Williford, R. E., & Hann, C. R. (1979). Effects of Fill Gas Composition and Pellet Eccentricity: Comparison Between Instrumented Fuel Assemblies IFA-431 and IFA-432 REFERENCE COPY.

Deng, Y., Shirvan, K., Wu, Y., Su, G., 2019. Utilization of 3D fuel modeling capability of BISON to derive new insights in performance of advanced PWR fuel concepts. J. Nucl. Mater. 516, 271–288. https://doi.org/10.1016/j.jnucmat.2019.01.032.

Eucken, A., 1940. Allgemeine Gesetzmäßigkeiten für das Wärmeleitvermögen verschiedener Stoffarten und Aggregatzustände. Forschung Auf Dem Gebiete Des Ingenieurwesens 11 (1), 6–20. https://doi.org/10.1007/BF02584103.

Fayette, L., Reboul, S., Robert, N., Hanifi, K., Bienvenu, P., Roure, I., Zacharie, I., Blay, T. S., Martin, L. F., Lacroix, B., Volle, G., Reverte, A., Blanc, V., Hautefeuille, J., Delion, P., & Silvestre Setc, P. (2022). Post Irradiation Examinations CAPRIX (MOX 45% Pu, fast spectrum, nominal conditions). www.cea.fr.

Generation IV International Forum. (2014). Technology roadmap update for generation IV nuclear energy systems. https://doi.org/10.2172/859105.

Geuzaine, C., Remacle, J.F., 2009. Gmsh: a 3-D finite element mesh generator with built-in pre- and post-processing facilities. Int. J. Numer. Meth. Eng. 79 (11), 1309–1331. https://doi.org/10.1002/nme.2579.

Hales, J.D., Perez, D.M., Williamson, R.L., Novascone, S.R., Spencer, B.W., Martineau, R. C., 2013. Validation of the BISON 3D fuel performance code. Temperature Comparisons for Concentrically and Eccentrically Located Fuel Pellets 37th Enlarged Halden Program Group Meeting.

Harayama, Y., Kyoya, M., 1986. Analysis of effect of eccentric holes in pellets on temperature and heat flux distribution in fuel rod. J. Nucl. Sci. Technol. 23 (2), 151–159. https://doi.org/10.1080/18811248.1986.9734962.

Harp, J. M., & Chichester, H. J. M. (2017). Fuel Cycle Research & Development Advanced Fuels Campaign Baseline Postirradiation Examination of Fuel Rodlets from the AFC-2C Experiment*. http://www.inl.gov.

Helfer, T., Bejaoui, S., Michel, B., 2015. Licos, a fuel performance code for innovative fuel elements or experimental devices design. Nucl. Eng. Des. 294, 117–136. https://doi.org/10.1016/j.nucengdes.2015.07.070.

Jaramillo-Sierra, D., Stefanowska-Skrodzka, M., Lavarenne, J., Deveaux, E., Brunetto, E., Matocha, V., Magni, A., Sturm, K., Mikityuk, K., Wang, Y., Jiménez-Carrascosa, A., Gado, J., Burger, B., Blanc, V., Dupont, V., Argeles, L., Perrin, B., Michel, G., Scolaro, A., Strmensky, C., 2025. PuMMA blind benchmark: Performance of high plutonium content MOX fuel under irradiation. Nucl. Eng. Des. 435. https://doi.org/10.1016/j.nucengdes.2025.113960.

Kato, M., Maeda, K., Ozawa, T., Kashimura, M., Kihara, Y., 2011. Physical properties and irradiation behavior Analysis of Np- and am-bearing MOX fuels. J. Nucl. Sci. Technol. 48 (4), 646–653. https://doi.org/10.1080/18811248.2011.9711745.

Lainet, M., Michel, B., Dumas, J.C., Pelletier, M., Ramière, I., 2019. GERMINAL, a fuel performance code of the PLEIADES platform to simulate the in-pile behaviour of mixed oxide fuel pins for sodium-cooled fast reactors. J. Nucl. Mater. 516, 30–53. https://doi.org/10.1016/J.JNUCMAT.2018.12.030.

Maeda, K., Katsuyama, K., Ikusawa, Y., Maeda, S., 2011. Short-term irradiation behavior of low-density americium-doped uranium-plutonium mixed oxide fuels irradiated in a fast reactor. J. Nucl. Mater. 416 (1–2), 158–165. https://doi.org/10.1016/j.jnucmat.2010.11.027.

Magni, A., Barani, T., Del Nevo, A., Pizzocri, D., Staicu, D., Van Uffelen, P., Luzzi, L., 2020. Modelling and assessment of thermal conductivity and melting behaviour of MOX fuel for fast reactor applications. J. Nucl. Mater. 541. https://doi.org/10.1016/j.jnucmat.2020.152410.

Magni, A., Del Nevo, A., Luzzi, L., Rozzia, D., Adorni, M., Schubert, A., & Van Uffelen, P. (2021). The TRANSURANUS fuel performance code. Nuclear power plant design and analysis codes: development, validation, and application, 161–205. https://doi.org/10.1016/B978-0-12-818190-4.00008-5.

Mcnary, O., & Bauer, T. H. (1981). The effect of asymmetric fuel-clad gap conductance on fuel pin thermal performance. In Nuclear Engineering and Design (Vol. 63).

Nijsing, R. (1966). Temperature and heat flux distribution in nuclear fuel element rods.

Novascone, S., Medvedev, P., Peterson, J.W., Zhang, Y., Hales, J., 2018. Modeling porosity migration in LWR and fast reactor MOX fuel using the finite element method. J. Nucl. Mater. 508, 226–236. https://doi.org/10.1016/j.jnucmat.2018.05.041.

Ozawa, T., Hirooka, S., Kato, M., Novascone, S., Medvedev, P., 2021. Development of fuel performance analysis code, BISON for MOX, named Okami: analyses of pore migration behavior to affect the MA-bearing MOX fuel restructuring. J. Nucl. Mater. 553. https://doi.org/10.1016/j.jnucmat.2021.153038.

Sens, P. F. (1972). The kinetics of pore movement in UO2 fuel rods.

Tao, Q., Zhang, B., Hui, Y., & Shan, J. (2023). Development and application of high-accuracy metal fuel performance analysis code based on fem method. Springer Proceedings in Physics, 284 SPPHY, 793–808. https://doi.org/10.1007/978-981-19-8780-9_77.

Van Til, S., Fedorov, A., & Charpin-Jacobs, F. (2021). Reconstruction of the irradiation history of TRABANT pin 2/2 PUMMA D2.1.3.

van Til, S., Fedorov, A.V., Nindiyasari, F., Charpin-Jacobs, F., Uitslag, G., Pasti, F., D'Agata, E., Chauvin, N., 2025. First Post Irradiation Examinations on a fast reactor grade MOX fuel (U0.6,Pu0.4)O2 for Pu-burning application, irradiated in the High Flux Reactor. J. Nucl. Mater. 608, 155707. https://doi.org/10.1016/J.JNUCMAT.2025.155707.

Van Til, S., Nindiyasari, F., & Fedorov, A. (2024). Post Irradiation Examinations on TRABANT pin 2/2 PUMMA D2.8.

Venard, C., & Deveaux, E. (2021). CAPRIX irradiation conditions in PHENIX D2.1.1.

Wiesenack, W. (1996). Separate effect studies at the halden reactor project related to fuel thermal performance and modelling.

Williamson, R.L., Gamble, K.A., Perez, D.M., Novascone, S.R., Pastore, G., Gardner, R.J., Hales, J.D., Liu, W., Mai, A., 2016. Validating the BISON fuel performance code to integral LWR experiments. Nucl. Eng. Design 301, 232–244. https://doi.org/10.1016/j.nucengdes.2016.02.020.

Williamson, R.L., Hales, J.D., Novascone, S.R., Pastore, G., Gamble, K.A., Spencer, B.W., Jiang, W., Pitts, S.A., Casagranda, A., Schwen, D., Zabriskie, A.X., Toptan, A., Gardner, R., Matthews, C., Liu, W., Chen, H., 2021. BISON: a flexible code for advanced simulation of the performance of multiple nuclear fuel Forms. Nucl. Technol. 207 (7), 954–980. https://doi.org/10.1080/00295450.2020.1836940.

Williford, R.E., Hann, C.R., 1977. Effects of Fill Gas Composition and Pellet Eccentricity Repart tn.